Numerical simulations of single-photon double ionization of the helium dimer

Hongcheng Ni,[1] Camilo Ruiz,[2] Reinhard Dörner,[3] and Andreas Becker[1]

[1]*JILA and Department of Physics, University of Colorado, Boulder, Colorado 80309-0440, USA*
[2]*Centro de Láseres Pulsados (CLPU), Edificio M3 Parque Científico C/ Adaja, s/n 37185 Villamayor, Spain*
[3]*Institut für Kernphysik, Johann Wolfgang Goethe Universität, Max-von-Laue-Straße 1, 60438 Frankfurt, Germany*

We study the energy exchange via electron correlation upon photon absorption over large distances in double photoionization of the helium dimer. Results of numerical simulations of the interaction of a planar helium dimer model with a short light pulse are found to be in good agreement with recent experimental data for the angular distribution of the emitted electron. The double ionization probability is closely related to that of the photoemission of an electron from one of the helium atoms along the internuclear axis. Together with an analysis of the temporal evolution of the two-electron probability distribution this provides direct evidence for the knockoff mechanism by which the photon energy is shared between the electrons over distances of several Angstroms in the dimer.

I. INTRODUCTION

Recent advances in experimental and theoretical studies of double photoionization of atoms and molecules [1–11] have contributed to our understanding of the correlated dynamics of charged particles, which is the basis of any chemical reaction. This has led to a profound understanding of the correlated emission of two electrons in light-induced double ionization of atoms. However, the role of electron correlation in double photoionization of a molecule, in particular, regarding the recently observed energy exchange between electrons over distances of several Angstroms [12], is less understood than in the atomic case. In this respect rare gas dimers, which are formed via the attractive van der Waals interaction by two atoms at larger equilibrium distances than those in a typical diatomic molecule, are interesting targets. Among them, the helium dimer is by far the most extended. Here, interatomic Coulombic decay (ICD) [13], as well as double photoionization [14], which are both mediated by electron-correlation effects, have been observed recently.

In double photoionization, the energy of a single photon absorbed from the light field is shared between two electrons, leading to the correlated emission of both electrons from the target. In a rare gas dimer, the two emitted electrons can originate either from the same atom or from different atoms. Due to the strong localization of electrons in the dimer, the minimum energy required for the emission of two electrons from different atoms in the dimer is about twice the energy for single ionization of the rare gas atom. For He_2, this minimum energy is about 49.2 eV, which is considerably smaller than the energy of about 79 eV needed for emission of both electrons from the same helium atom in the dimer. The threshold for ionization plus excitation (to the $n = 2$ state) in He is 65.4 eV. Below this threshold ICD as a double ionization channel is closed. By selecting a photon energy of 49.2 eV $< \hbar\omega <$ 65.4 eV, one can therefore study electron-correlation effects in double photoionization of the helium dimers over a bond length of more than 5 a.u. which are not ICD related. Recent experimental data suggest that the emission of the two electrons in this case proceeds as follows [14]: A primary electron localized at one atom in the helium dimer absorbs the photon energy from the field, then propagates along the internuclear axis and transfers its energy to a second electron in the neighboring helium atom. This process is called *knockoff* in view of the close analogy to a similar mechanism known in double photoionization of atoms [15]. Since the atoms in the helium dimer are well separated it was further argued [14] that in this case the knockoff process can be considered as the photoionization of a helium atom followed by a subsequent electron-impact ionization at the other helium atom in the dimer. This interpretation was supported by a comparison of the experimental data with theoretical results for electron-impact ionization of the helium atom.

In this paper, we analyze the experimental data and the underlying mechanism for double photoionization of the helium dimer via time-dependent *ab initio* numerical simulations. To this end, in Sec. II we propose a two-active-electron model for the dimer, in which one electron at each atom is considered to be active. The motion of the two electrons is restricted to a plane and, in view of the ultrafast dynamics of the electrons, the positions of the residual ions are kept frozen over the interaction with the XUV laser pulse. In Sec. III we then present comparisons of the predictions of the theoretical model with recent experimental data [14] for the photoelectron angular distributions. Based on the good agreement between experimental and theoretical data we then proceed in Sec. IV to provide evidence, based on predictions for the dependence of the ionization signals on the orientation of the dimer axis and the separation of the atoms in the dimer, and a real-time visualization of the knockoff mechanism behind the long-range electron correlation. The paper ends with concluding remarks.

II. NUMERICAL SIMULATIONS

In this section we present the numerical model for the helium dimer used in the simulations, in which one electron at each atom in the dimer is considered as being active. We further outline the methods used in the numerical simulations and then present the predictions for the lowest energy eigenstates based on this numerical model.

A. Numerical model of the helium dimer

A solution of the Schrödinger equation including the dynamics of all six charged particles and the interaction of all four electrons with the external light field is currently not conceivable. We therefore propose a planar two-active-electron model of the helium dimer, in which the electrons are located at different atoms in the dimer and their dynamics is constrained to the same plane, as shown schematically in Fig. 1. Such a model excludes ICD but it is well suited to treat the knockoff mechanism. The orientation of the dimer axis is chosen to be at an angle θ to the axis of linear polarization of the light field (here, the z axis). It is further assumed that the correlated emission of the two electrons proceeds fast enough (a few tens of attoseconds, 1 as $= 10^{-18}$ s) to hold the internuclear distance between the atoms as well as the orientation of the dimer axis fixed in space during the

simulation. The corresponding four-dimensional (two spatial dimensions for each electron) model Hamiltonian is then given by (Hartree atomic units, $e = m_e = \hbar = 1$, are used in the remainder of the article)

$$
\begin{aligned}
H = {} & \frac{p_{x_1}^2 + p_{z_1}^2}{2} + \frac{p_{x_2}^2 + p_{z_2}^2}{2} + E(t)(z_1 + z_2) \\
& + V_{\mathrm{SAE}}(r_{11}) + V_{\mathrm{SAE}}(r_{12}) + V_{\mathrm{SAE}}(r_{21}) + V_{\mathrm{SAE}}(r_{22}) \\
& + \frac{1}{\sqrt{(x_1 - x_2)^2 + (z_1 - z_2)^2 + b^2}} + \frac{1}{R},
\end{aligned}
\tag{1}
$$

where $\boldsymbol{p}_i = (p_{x_i}, p_{z_i})$ and $\boldsymbol{r}_i = (x_i, z_i)$ (with $i = 1,2$) are the momentum operators and spatial coordinates of the two active electrons and $E(t)$ is the laser field, which is assumed to be linearly polarized in the z direction. R is the internuclear distance that can have different orientations θ with respect to the polarization direction and

$$
r_{ij} = \sqrt{\left(x_i + \frac{(-1)^j R}{2} \sin\theta \right)^2 + \left(z_i + \frac{(-1)^j R}{2} \cos\theta \right)^2 + a^2}
\tag{2}
$$

corresponds to the distance between ith electron and jth nucleus ($i, j = 1,2$) with $a^2 = 0.201$ and $b^2 = 0.01$ denoting soft-core parameters.

$$
V_{\mathrm{SAE}}(r) = -\frac{Z_c + a_1 e^{-a_2 r} + a_3 r e^{-a_4 r} + a_5 e^{-a_6 r}}{r}
\tag{3}
$$

is a single-active-electron (SAE) potential for the helium atom with $Z_c = 1.0$, $a_1 = 1.231$, $a_2 = 0.662$, $a_3 = -1.325$, $a_4 = 1.236$, $a_5 = -0.231$, and $a_6 = 0.480$ [16], which we adopt here for the planar case. The time-dependent Schrödinger equation of this four-dimensional (4D) model is solved numerically using the Crank-Nicolson method on a grid with $N_{x_1} = N_{x_2} = 200$ and $N_{z_1} = N_{z_2} = 300$ grid points, a grid step of $\Delta x_1 = \Delta x_2 = \Delta z_1 = \Delta z_2 = 0.3$, and a time step of $\Delta t = 0.05$.

In our simulations we considered double photoionization due to the interaction of the model helium dimer with a
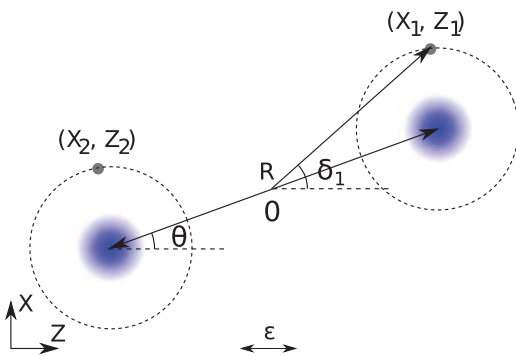

FIG. 1. (Color online) Scheme of the numerical model for the helium dimer. One electron at each atom is considered active and restricted to the same plane, with coordinates (x_1, z_1) and (x_2, z_2), respectively. The internuclear distance R and dimer orientation θ with respect to the laser polarization direction ε (z axis) are fixed during the simulations.

four-cycle XUV light pulse at a central wavelength of 20 nm (corresponding to a photon energy of 62 eV and a bandwidth of ± 15.5 eV) and a peak intensity of 1×10^{14} W/cm^2. At this bandwidth in a real four-electron system, the ICD channel would be open for the high-energy tail of the pulse. In our two-electron calculations, however, ICD is excluded and hence does not obscure our findings. We employed absorbing boundaries of the form $\cos^{1/6}(\frac{\pi}{2} \frac{|x - x_0|}{L})$ with $|x| \geqslant |x_0|$, where x_0 denotes the border of the boundary region and L is its width. The boundary was chosen to span 10% of the grid size in each direction. In order to calculate the total probabilities and electron angular distributions, we stopped the simulation before the respective part of the wave function reached the boundaries.

In order to analyze the correlated electron emission from the helium dimer and to compare with the experimental data on the photoelectron angular distributions, the contributions to single and double photoionization of the helium dimer were obtained by partitioning the spatial four-dimensional grid. To this end, we identified the neutral helium dimer contributions as those where both electrons remain either centered within a distance of $d_{\mathrm{neutral}} = 7$ a.u. at different nuclei in the dimer or in the region between the two nuclei and within a transverse distance of $d_{\mathrm{neutral}} = 7$ a.u. Singly ionized contributions are identified by requiring that one of the two electrons remains in regions of the same shape but with $d_{\mathrm{single}} = 4$ a.u. The complementary part of the space was identified as double ionization. In test calculations we varied the regions and distances chosen to validate the general conclusions drawn below.

B. Initial states

The lowest energy eigenstates of the model, which we used as initial states for our numerical simulations, are obtained via imaginary time propagation. For an internuclear separation of 5.6 a.u., which corresponds to the minimum of the helium dimer potential [17], and orientation of the dimer along the z
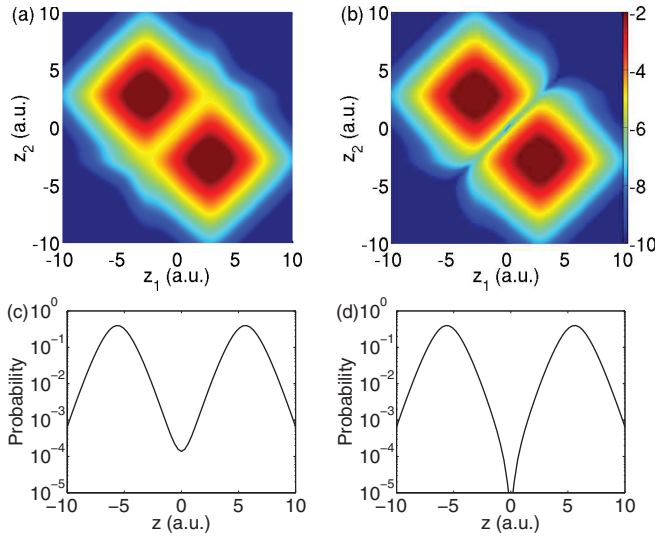
FIG. 2. (Color online) Spatial distributions (on a logarithmic scale) of the ground state [panels (a) and (c)] and first excited state [panels (b) and (d)] of the planar model helium dimer. The distributions in the upper row are integrated over x_1 and x_2 and shown as a function of z_1 and z_2. The distributions in the lower row are integrated over x_1, x_2, and $Z = \frac{z_1 + z_2}{2}$ and shown as a function of $z = z_1 - z_2$. Note the node at $z_1 = z_2$ or $z = 0$ in the distributions of the first excited state.

axis, spatial distributions of the two lowest energy eigenstates are shown in Fig. 2 as functions of z_1 and z_2 (upper row) and $z = z_1 - z_2$ (lower row), respectively. The distributions are integrated over the other coordinates. Due to the large internuclear distance the states are, as expected, very close in energy (-1.80740 a.u. and -1.80726 a.u., respectively), with values close to other theoretical calculations [18]. Note the emergence of these two separate states is due to our two-active-electron model that selects two electrons out of a total of four. The ground state is a spin-singlet state which has a multiplicity of 1 while the first excited state is a spin-triplet state with a multiplicity of 3. We performed separate simulations for both states as the initial state and present below, if not mentioned differently, the sum of the contributions by taking account of the multiplicity of each state.

III. PHOTOELECTRON ANGULAR DISTRIBUTIONS

Angular electron-momentum distributions for double photoionization were obtained by projection of the respective spatial part of the wave function onto an approximate final-state wave function. We expressed the Coulomb potential between the two electrons and the residual ions as well as among the electrons in the center of mass [c.m., $X = (x_1 + x_2)/2$ and $Z = (z_1 + z_2)/2$] and relative coordinates ($x = x_1 - x_2$ and $z = z_1 - z_2$) of the two electrons, as

$$V = -\sum_{i,j=1}^{2} \left[\left(X - (-1)^i \frac{x}{2} + (-1)^j \frac{R}{2} \sin\theta \right)^2 \right.$$
$$\left. + \left(Z - (-1)^i \frac{z}{2} + (-1)^j \frac{R}{2} \cos\theta \right)^2 \right]^{-1/2} + \frac{1}{\sqrt{x^2 + z^2}}. \tag{4}$$

For $X, Z, R \gg x, z$, this potential reduces to

$$V \approx \frac{1}{\sqrt{x^2 + z^2}}, \tag{5}$$

which suggests to approximate the final state as a product of a Coulomb wave in the relative and a plane wave in the c.m. coordinates. Since our model is planar, we used a two-dimensional Coulomb wave [19,20].

In view of the dimensional restrictions of our model as well as the projection of the final-state wave function onto an approximative two-electron continuum wave function we first test the theoretical model predictions against recent experimental data. To this end, we present in Fig. 3 a comparison of the results (solid lines) for the molecular-frame angular distribution of one of the electrons following double photoionization from our model simulations for $R = 5.6$ a.u.
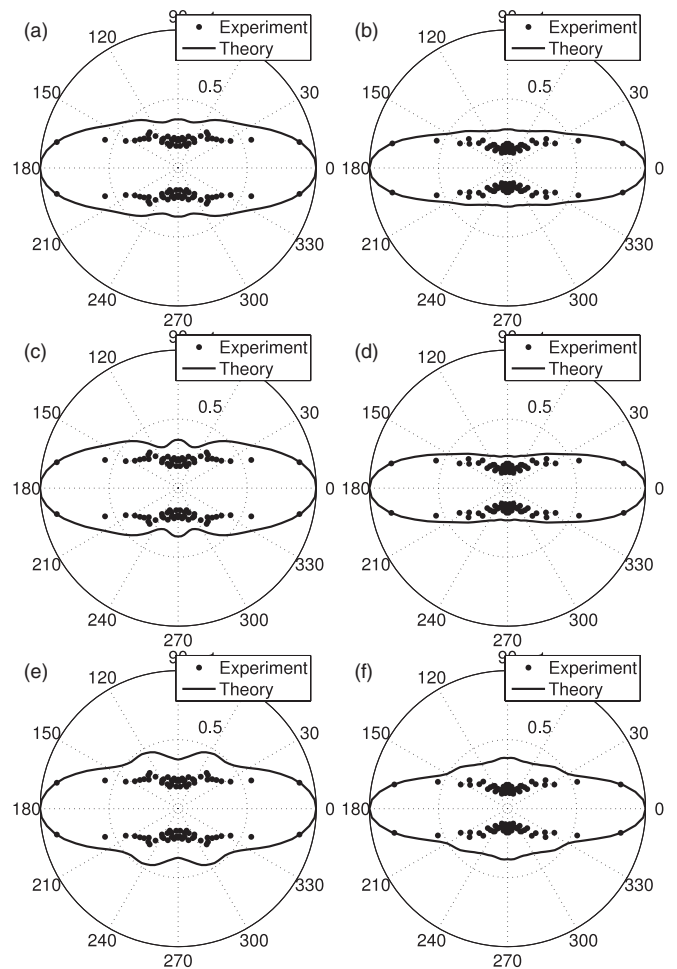

FIG. 3. Molecular-frame angular distribution of one of the electrons following double ionization of the helium dimer model with internuclear distances of $R = 5.6$ a.u. [panels (a), (c), and (e)] and $R = 10$ a.u. [panels (b), (d), and (f)] by a 20-nm, 4-cycle XUV pulse with a peak intensity of 1×10^{14} W/cm^2. Shown is a comparison between the theoretical results [solid lines, full results in panels (a) and (b), singlet contributions in panels (c) and (d), and triplet contributions in panels (e) and (f)] and the experimental data [solid circles, integrated over $R = 5.1-6.8$ a.u. in panels (a), (c), and (e), and $R = 9.4-10.9$ a.u. in panels (b), (d), and (f)] (subset of data shown in Fig. 3(b) of Ref. [14]).

[Figs. 3(a), 3(c), and 3(e)] and $R = 10$ a.u. [Fig. 3(b), 3(d), and 3(f)] with the experimental data (solid circles, Ref. [14]). The distributions represent the probabilities for emission of one of the two electrons at an angle δ to the dimer axis and are integrated over the emission angle of the second electron as well as the energies of the electrons. In panels (a) and (b), the results for the (weighted) sum of singlet and triplet states are shown, while in the other panels the contributions for the singlet [panels (c) and (d)] and the triplet [panels (e) and (f)] states are presented separately. In order to compare with the experiment, the theoretical results are calculated for different axis orientations and then averaged, and have been mirrored with respect to the position of the two atoms in the dimer and matched to coincide with the experimental data at the maximum of the distributions. The comparison shows an overall good agreement between the theoretical and experimental angular profiles.

IV. THE KNOCKOFF MECHANISM

On the basis of the comparison presented in Fig. 3, we proceed to obtain insights into the mechanism of the correlated electron emission from the helium dimer. As mentioned at the outset, it was argued based on the experimental data and a comparison with theoretical results from electron-impact ionization that the double photoionization proceeds via a knockoff-type mechanism. According to this mechanism the double ionization probability should be closely related to the probability that the primary photoelectron, launched at one helium atom, "hits" the second electron, which is localized in the neighboring atom. The results in Figs. 4 and 5 confirm this close relation based on our theoretical data, which provides strong evidence for the knockoff mechanism.

First, we compare in Fig. 4(b) the probability of double photoionization as a function of the orientation of the dimer axis with respect to the polarization direction of the field (solid

FIG. 5. Double photoionization probability (open circles) as a function of internuclear distance R for orientation of the dimer axis parallel to the polarization direction of the field. It scales as $1/R$ with the internuclear distance. The fitting parameters are $a = 2.88 \times 10^{-5}$ and $b = -4.56 \times 10^{-7}$. The parameters of the XUV field are the same as in Fig. 3.

line) with the experimental data (solid circles [14]) and a $\cos^2 \delta$ distribution (dash-dotted line). The comparison shows not only an excellent agreement between theoretical predictions and experimental data but moreover indicates a close relation between the double ionization probability and the direction of the primary photoelectron momentum. The latter is close to the expected p-wave (or $\cos^2$) distribution as can be seen from the theoretical results in panel (a) for orientation of dimer axis parallel (red [gray] solid line) as well as perpendicular (blue [gray] dashed line) to the polarization direction of the field. The small deviation from the $\cos^2$ distribution in the case of parallel orientation indicates the effect of elastic scattering of the photoelectron at the second atom in the single ionization data, in agreement with similar observations for the neon dimer [21].

Further evidence for the knockoff mechanism is given by the dependence of the double photoionization probability on the internuclear distance R. For the knockoff mechanism, the probability of the primary photoelectron "hitting" the second electron that produces double ionization is expected to decrease with an increase of R, since the wavepacket representing the primary photoelectron expands in space. Our theoretical results for the double photoionization probability, shown in Fig. 5, indeed follow closely the expected $1/R$ trend for the case of parallel orientation of the dimer axis in our planar model. We may emphasize that in the real three dimensional (3D) helium dimer we expect an even stronger $1/R^2$ decrease. We may further note that the double-to-single ionization ratio follows the same trend as the double photoionization probability.

Moreover, our time-dependent simulations provide a "movie" of the scattering process as a function of time. During the knockoff process, it is expected that one of the electrons approaches the other after the initial absorption of the photon. This can be visualized via the temporal evolution of the two-electron probability distribution as a function of the relative coordinate $z = z_1 - z_2$ along the polarization direction. The respective results of our numerical simulations for an internuclear distance of 15 a.u. are shown in Fig. 6.
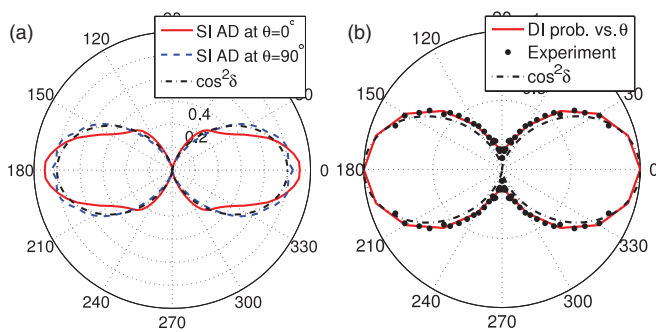

FIG. 4. (Color online) Comparison of the laboratory-frame dipole-transition angular distribution $\cos^2 \delta$ (dashed-dotted line) with (a) the theoretical photoelectron angular distributions (AD) for single ionization (SI) of the dimer oriented either parallel (red [gray] solid line) or perpendicular (blue [gray] dashed line) to the polarization axis and (b) the probability of double photoionization (DI) as a function of the orientation of the dimer axis (theoretical prediction: red [gray] solid line, experimental data: solid circles, integrated over $R = 4.5 - 6.8$ a.u. (subset of data shown in Fig. 3(a) of Ref. [14])). The polarization direction of the field is along the horizontal axis in both panels. The internuclear distance was chosen to be $R = 5.6$ a.u. and the parameters of the XUV field are the same as in Fig. 3.
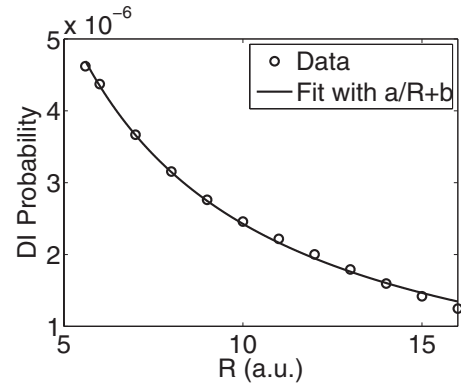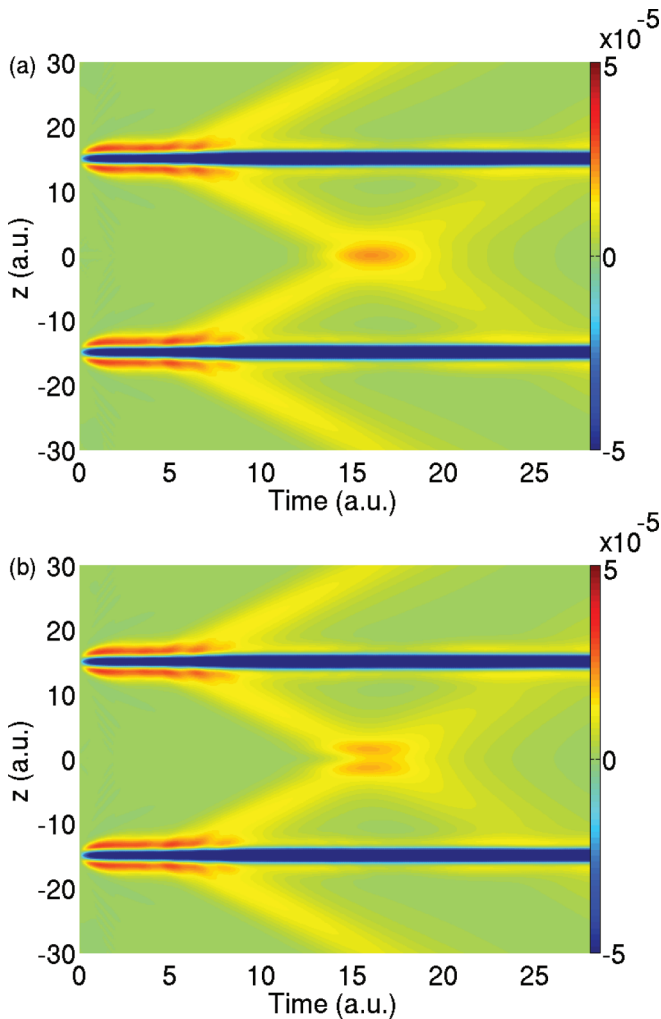
FIG. 6. (Color online) Temporal evolution of the two-electron probability distribution of the helium dimer in $z = z_1 - z_2$ starting from the ground state [singlet, panel (a)] and the first excited state [triplet, panel (b)], which exhibit the differences between singlet and triplet scattering. In the simulation, the dimer axis is oriented parallel to the polarization axis.

The initial-state probability distribution, localized at the two nuclei, has been subtracted in order to enhance the visibility of the small contributions leading to single and double ionization. The results for the temporal evolution starting from the ground state [singlet, panel (a)], and the first excited state [triplet, panel (b)] confirm our previous conclusions regarding the knockoff mechanism. The exchange asymmetry in the wave function of the triplet state illustrates itself as a minimum at $z = 0$, which is particularly apparent when the two electrons are close to

each other. Due to the integration over x_1 and x_2, we observe a minimum in the distributions instead of a node, which would show up at fixed transverse distances.

V. CONCLUDING REMARKS

In conclusion, we have proposed a planar two-active-electron model to analyze the recently observed correlation effects in double photoionization of the helium dimer. Results of numerical simulations for the angular distribution of the electron are found to be in good agreement with the experimental data. Furthermore, theoretical predictions for the double ionization probability as functions of the orientation of the dimer axis as well as the distance of the atoms in the dimer reveal direct evidence for the knockoff mechanism, in which the photon energy is transferred over distances of several Angstroms in the dimer to be shared between the electrons. Our conclusions are further supported by an analysis of the temporal evolution of the two-electron probability distribution. An analogous situation to the one discussed here for the helium dimer is encountered in the creation of two-site double core holes of molecules [22,23] discovered recently. Here the photon is absorbed at one K shell, e.g., in the C_2H_2 molecule [23]. The two K shells have almost negligible overlap and their spatial separation is much bigger than the extension of the individual K shell itself. Hence we expect that the conclusions drawn from our calculations are also valid for the case of single-photon-induced two-site double-core-hole production.

[1] R. Wehlitz, F. Heiser, O. Hemmers, B. Langer, A. Menzel, and U. Becker, Phys. Rev. Lett. **67**, 3764 (1991).

[2] O. Schwarzkopf, B. Krässig, J. Elmiger, and V. Schmidt, Phys. Rev. Lett. **70**, 3008 (1993).

[3] F. Maulbetsch and J. S. Briggs, J. Phys. B **26**, 1679 (1993).

[4] A. S. Kheifets and I. Bray, J. Phys. B **31**, L447 (1998).

[5] C. Ruiz, L. Plaja, L. Roso, and A. Becker, Phys. Rev. Lett. **96**, 053001 (2006).

[6] D. Akoury, K. Kreidi, T. Jahnke, T. Weber, A. Staudte, M. Schöffler, N. Neumann, J. Titze, L. P. H. Schmidt, A. Czasch, O. Jagutzki, R. A. Costa Fraga, R. E. Grisenti, R. Díez Muiño, N. A. Cherepkov, S. K. Semenov, P. Ranitovic,

C. L. Cocke, T. Osipov, H. Adaniya, J. C. Thompson, M. H. Prior, A. Belkacem, A. L. Landers, H. Schmidt-Böcking, and R. Dörner, Science **318**, 949 (2007).

[7] R. Dörner, H. Bräuning, O. Jagutzki, V. Mergel, M. Achler, R. Moshammer, J. M. Feagin, T. Osipov, A. Bräuning-Demian, L. Spielberger, J. H. McGuire, M. H. Prior, N. Berrah, J. D. Bozek, C. L. Cocke, and H. Schmidt-Böcking, Phys. Rev. Lett. **81**, 5776 (1998).

[8] C. Siedschlag and T. Pattard, J. Phys. B **38**, 2297 (2005).

[9] W. Vanroose, D. A. Horner, F. Martín, T. N. Rescigno, and C. W. McCurdy, Phys. Rev. A **74**, 052702 (2006).

[10] S. Baier, C. Ruiz, L. Plaja, and A. Becker, Phys. Rev. A **74**, 033405 (2006).

[11] J. Colgan, M. S. Pindzola, and F. Robicheaux, Phys. Rev. Lett. **98**, 153001 (2007).

[12] T. Hartman, P. N. Juranić, K. Collins, B. Reilly, N. Appathurai, and R. Wehlitz, Phys. Rev. Lett. **108**, 023001 (2012).

[13] T. Havermeier, T. Jahnke, K. Kreidi, R. Wallauer, S. Voss, M. Schöffler, S. Schössler, L. Foucar, N. Neumann, J. Titze, H. Sann, M. Kühnel, J. Voigtsberger, J. H. Morilla, W. Schöllkopf, H. Schmidt-Böcking, R. E. Grisenti, and R. Dörner, Phys. Rev. Lett. **104**, 133401 (2010).

[14] T. Havermeier, T. Jahnke, K. Kreidi, R. Wallauer, S. Voss, M. Schöffler, S. Schössler, L. Foucar, N. Neumann, J. Titze, H. Sann, M. Kühnel, J. Voigtsberger, A. Malakzadeh, N. Sisourat, W. Schöllkopf, H. Schmidt-Böcking, R. E. Grisenti, and R. Dörner, Phys. Rev. Lett. **104**, 153401 (2010).

[15] J. A. R. Samson, Phys. Rev. Lett. **65**, 2861 (1990).

[16] X. M. Tong and C. D. Lin, J. Phys. B **38**, 2593 (2005).

[17] R. A. Aziz and M. J. Slaman, J. Chem. Phys. **94**, 8047 (1991).

[18] W. Cencek and K. Szalewicz, Int. J. Quant. Chem. **108**, 2191 (2008).

[19] L. S. Davtyan, G. S. Pogosyan, A. N. Sisakyan, and V. M. Ter-Antonyan, Theor. Math. Phys. **74**, 157 (1988).

[20] X. L. Yang, S. H. Guo, F. T. Chan, K. W. Wong, and W. Y. Ching, Phys. Rev. A **43**, 1186 (1991).

[21] T. Jahnke, A. Czasch, M. Schöffler, S. Schössler, M. Käsz, J. Titze, K. Kreidi, R. E. Grisenti, A. Staudte, O. Jagutzki, L. P. H. Schmidt, S. K. Semenov, N. A. Cherepkov, H. Schmidt-Böcking, and R. Dörner, J. Phys. B **40**, 2597 (2007).

[22] L. S. Cederbaum, F. Tarantelli, A. Sgamellotti, and J. Schirmer, J. Chem. Phys. **85**, 6513 (1986).

[23] P. Lablanquie, T. P. Grozdanov, M. Žitnik, S. Carniato, P. Selles, L. Andric, J. Palaudoux, F. Penent, H. Iwayama, E. Shigemasa, Y. Hikosaka, K. Soejima, M. Nakano, I. H. Suzuki, and K. Ito, Phys. Rev. Lett. **107**, 193004 (2011).